Molecular Cancer Therapeutics

Necuparanib, A Multitargeting Heparan Sulfate Mimetic, Targets Tumor and Stromal Compartments in Pancreatic Cancer

Amanda MacDonald[1], Michelle Priess[1], Jennifer Curran[1], Jamey Guess[1], Victor Farutin[1], Ilse Oosterom[2], Chia Lin Chu[1], Edward Cochran[1], Lynn Zhang[1], Kristen Getchell[1], Martijn Lolkema[2], Birgit C. Schultes[1], and Silva Krause[1]

Abstract

Pancreatic cancer has an abysmal 5-year survival rate of 8%, making it a deadly disease with a need for novel therapies. Here we describe a multitargeting heparin-based mimetic, necuparanib, and its antitumor activity in both *in vitro* and *in vivo* models of pancreatic cancer. Necuparanib reduced tumor cell proliferation and invasion in a three-dimensional (3D) culture model; *in vivo*, it extended survival and reduced metastasis. Furthermore, proteomic analysis demonstrated that necuparanib altered the expression levels of multiple proteins involved in cancer-driving pathways including organ development, angiogenesis, proliferation, genomic stability, cellular energetics, and invasion and metastasis. One protein family known to be involved in invasion and metastasis and altered by necuparanib treatment was the matrix metalloprotease (MMP) family. Necuparanib reduced metalloproteinase 1 (MMP1) and increased tissue inhibitor of metalloproteinase 3 (TIMP3) protein levels and was found to increase RNA expression of TIMP3. MMP enzymatic activity was also found to be reduced in the 3D model. Finally, we confirmed necuparanib's *in vivo* activity by analyzing plasma samples of patients enrolled in a phase I/II study in patients with metastatic pancreatic cancer; treatment with necuparanib plus standard of care significantly increased TIMP3 plasma protein levels. Together, these results demonstrate necuparanib acts as a broad multitargeting therapeutic with *in vitro* and *in vivo* anti-invasive and antimetastatic activity.

Introduction

Pancreatic cancer is a devastating disease with a high unmet need for effective therapies. The 5-year survival rate of 8% is one of the lowest for any cancer and has only slightly improved over the last decade (1, 2). Over 80% of patients with pancreatic cancer have advanced metastatic disease at diagnosis, which has few therapies and low survival rates (3–5). As projections suggest that the incidence of pancreatic cancer will increase in the next decade, the need for novel therapies will also increase (6).

The intrinsic resistance of pancreatic tumors to treatment is the biggest challenge for novel drug development. Resistance is driven by stromal components, which can constitute up to 90% of a pancreatic tumor and are hypothesized to create both biological and physical impediments to treatment (7, 8). Biologically the stroma is hypothesized to impede treatment by promoting aberrant signaling. During tumorigenesis, the extracellular matrix (ECM) becomes dysregulated, promoting tumor transformation and metastasis and promoting stromal dysregulation, increasing angiogenesis and inflammation. Physically, the abundant stroma creates a barrier hypothesized to impede treatment by preventing therapeutic agents like chemotherapies and immune cells from entering the tumor (8–10), although recent research has shown that ablating the stromal compartment can both enhance and decrease tumor growth (11–13). Thus, while further research is needed to decipher its role, current stromal-targeting therapies are shifting to focus on reducing stromal dysregulation rather than stromal ablation (14, 15). Ideally, novel pancreatic cancer therapies would overcome tumor resistance by targeting both tumor growth and stromal dysregulation simultaneously.

Necuparanib, a heparin mimetic, is rationally designed to have reduced anticoagulation activity while retaining the ability to bind and sequester multiple heparin-binding growth factors, chemokines, and adhesion molecules key to cancer progression (16). By binding and sequestering different proteins, necuparanib acts as a multitargeting therapeutic, altering multiple signaling pathways simultaneously. We have previously reported an in-depth analysis of necuparanib's properties, including an over 10-fold reduction anti-coagulation and various antitumor properties, among them a reduction in angiogenesis, tumor burden, and tumor metastasis in a breast cancer model and in several metastases models (16).

Many of the pathways driving tumor growth and stromal dysregulation in pancreatic cancer are heparan sulfate–dependent and can be modulated by necuparanib. Here we investigated the ability of necuparanib to simultaneously inhibit tumor growth and stromal dysregulation in *in vitro* and *in vivo* models of pancreatic cancer and demonstrated that necuparanib not only reduced tumor cell proliferation but also modulated the tumor

[1]Momenta Pharmaceuticals, Inc. Cambridge, Massachusetts. [2]Erasmus Medical Center Cancer Center, Erasmus Medical Center, Rotterdam, the Netherlands.

Note: Supplementary data for this article are available at Molecular Cancer Therapeutics Online (http://mct.aacrjournals.org/).

Corresponding Author: Silva Krause, Momenta Pharmaceuticals, 301 Binney Street, Cambridge, MA 02142. Phone: 617-715-3682; Fax: 617-621-0431; E-mail: silvakrause@hotmail.com

doi: 10.1158/1535-7163.MCT-18-0417

microenvironment by altering multiple pathways and protein families.

Materials and Methods

Reagents and cell lines

Gemcitabine was purchased from Accord Healthcare and GM6001 (17) from EMD Millipore. Pancreatic cancer line AsPC-1 was purchased from ATCC and human pancreatic stellate cells (PSC) from ScienCell.

Necuparanib (formerly M402), M202 (an N-desulfated derivative), and the n-desulfated necuparanib derivative M202 were prepared as described previously (16). Labeled necuparanib was prepared by coupling either HiLyte Fluor 488 Hydrazide or HiLyte Fluor 750 Hydrazide (AnaSpec) to necuparanib in the presence of 1-ethyl-3-(3-dimethylaminopropyl) carbodiimide (EDC, Sigma-Aldrich Chemicals) and isolated by salt–methanol precipitation.

GEMM mouse model

Conditional LSL-Trp53R172H/+, Trp53Flox (18), LSL-KrasG12D/+, Pdx-Cre (19) strains were interbred to generate LSL-KrasG12D/+; LSL-Trp53R172H/Flox; Pd-Cre KPFMC triple mutant and LSL- on a mixed 129/SvJae/C57Bl/6 and 129/SvJae/C57Bl/6/FVB background. Tumor development in this model starts on day 30. For overall survival studies of KPFMC mice, necuparanib (40 mg/kg/day) or saline treatment was started on day 30 after birth, administered by osmotic pumps (OP, Alzet model 1004, Durect Corporation) implanted subcutaneously into all mice. On day 30, treatment with gemcitabine (50 mg/kg, twice weekly, intraperitoneal (i.p.) injection) was also started. KPFMC mice were examined three times per week for overall health and sacrificed when they showed piloerection, diarrhea, and/or abdominal enlargement from ascites (clinical endpoint). Survival odds were compared with a Cox proportional hazards model. Soft-tissue metastasis was determined by step sectioning of isolated and fixed liver and lungs and compared using Fisher exact test. All animal procedures are in agreement with current Dutch Law on animal experiments and were approved by the UMC Utrecht Animal Care Ethics Committee.

Cell culture

AsPC-1 cells were cultured from thaw up to 10 passages in RPMI1640 medium (ATCC), both with 10% FBS (v/v, HyClone). PSCs were cultured from thaw up to six passages in stellate complete medium (ScienCell). All cells were maintained at 37°C and 5% CO_2 and passaged using 0.05% trypsin (HyClone). All cell lines were tested for *Mycoplasma* contamination every 6 months.

3D spheroid culture and fluorescent imaging

3D spheroids were cultured using Culturex 3D Spheroid Cell Invasion Assay kits (Trevigen) as per the manufacturer's instructions. For coculture spheroids, 3,000 AsPC-1 cells and 9,000 PSCs were used and 3,000 AsPC-1 cells were used in monocultures. Dosing concentrations were optimized independently for each spheroid and treatment type in replicate experiments; optimum doses were used in comparative and combination experiments. In particular, higher doses of gemcitabine were needed to achieve similar reduction in spheroid growth for coculture spheroids compared with monoculture spheroids. This is consistent with reports in the literature that fibroblasts increase gemcitabine resistance in cancer cells (20). For coculture experiments, a combined medium (1:1 RPMI1640:Stellate cell medium) was used. Spheroids were harvested on day 7 and fixed in 4% paraformaldehyde (w/v, Electron Microscopy Sciences) for 2–4 hours. Three to four biological replicate experiments were analyzed for each treatment; each biological replicate was composed of 6–8 technical replicates (spheroids) per condition.

Spheroids (3–6 replicates per treatment) were processed as paraffin blocks for histologic analyses. Each well containing spheroid and matrix of a 96-well plate was stained with toluene blue and then embedded into a 1.5% agarose gel (w/v) in a 12-well plate to facilitate sectioning, paraffin embedded, and sectioned. Sections (5 μm) were stained for proliferation using a monoclonal rat Ki67 antibody (eBioscience). Apoptotic cells were stained using a TUNEL Staining Kit (Roche Applied Science).

Live cell tracing studies were performed using CellTracker products (red (CMTPY) and green (CMFDA), Thermo Fisher Scientific) according to the manufacturer's instructions.

For spheroid experiments tracing necuparanib, HiLyte Fluor 488–labeled necuparanib was used to treat spheroids. Necuparanib's location was visualized using a confocal Leica TCS SP5 system (Leica Microsystems). The spheroids were scanned with a 25× objective lens, and 8-bit depth images with a resolution of up to 2048 × 2048 pixels were taken.

For experiments using dye-quenched collagen I and gelatin (DQ-collagen I, DQ-gelatin, from Thermo Fisher Scientific), the DQ substrate was dissolved in water (HyClone) at 3 mg/mL and incorporated into the normal invasion matrix at a 1:9 ratio.

3D spheroid morphometric analysis

Spheroid morphology was quantified using 2D images taken on days 3 and 7. Each image was analyzed using ImageJ software (NIH, Bethesda, MD) to determine total spheroid area and spheroid perimeter (21).

Treatment effects were quantified by spheroid outgrowth and circularity. Outgrowth was the change in spheroid area during treatment (day 7 −day 3). Using the final spheroid area and perimeter, the circularity, a measure of the object's deformation compared wiith a circle (22), was calculated as:

$$\text{Circularity} = 4\pi \times \frac{(\text{Area})}{(\text{Perimeter}^2)}$$

Proteomic and RNA analysis of 3D culture supernatants

Supernatant isolated from cocultured spheroids (3 per group) was analyzed using the SomaLogic SOMAscan aptamer-based high-density array proteomic platform (23). All supernatants were collected, randomized, and analyzed in parallel for 1,310 different analytes. Log base 2–transformed hybridization and quantile–quantile normalized data were used to compare protein levels; levels were insensitive to different normalization methods. *P* values were generated using the limma package in R (24) and any analyte with a Benjamini–Hochberg adjusted *P* value less than 0.05 was considered significantly altered. A Gene Ontology analysis was then performed using these results with the topGO package in R (25). GO terms were checked for overlap with analyzed proteins; enrichment of GO categories with significantly altered proteins was assessed by Fisher exact test and then ranked by *P* value.

For RNA expression, imbedded cocultured spheroids were isolated from invasion assay matrix by incubation on ice in Cell

Recovery Solution (1 mL per mL of gel, Corning). Pellets of isolated spheroids were extracted in RLT buffer using an RNeasy Mini Kit (Qiagen) analyzed for quality (Tapestation, Agilent), normalized, and subjected to reverse transcription using ProtoScript II Reverse Transcriptase (New England Biolabs). qPCR was performed (Roche LightCycler 480 II, Roche) and normalized expression values were derived from the second derivative max method of the crossing point ($\Delta\Delta C_p$).

Protein analysis of patient plasma

Plasma samples were obtained from patients enrolled in a publicly registered clinical trial of necuparanib in pancreatic cancer (clinicaltrials.gov, trial registration ID: NCT01621243) conducted in accordance with the guidelines for Good Clinical Practice and the Declaration of Helsinki; the Institutional Review Board at each enrolling institution approved the study and written informed consent was obtained from all patients. Blood samples were collected into EDTA-treated tubes, centrifuged at 1,300 × *g* for 10 minutes, and the plasma aliquoted and stored at −80°C at the start of each treatment cycle (4 weeks long). For analysis, samples were thawed on ice overnight, stored at 4°C, and used in ELISA kits (R&D Systems) as per kit instructions within 72 hours. Protein levels were normalized to total protein content (Pierce BCA Protein Assay Kit, Thermo Fisher Scientific). Changes in MMP levels were compared using the lme4 package (a linear mixed effects model) in R (26), accounting for the correlation between repeated measurements coming from the same patients. Conclusions reached with time treated as a continuous variable were the same as when time was treated as a categorical variable.

Statistical analysis

Unless otherwise noted, Prism (GraphPad Software) was used for all statistical analyses. Comparison of time points within a single treatment was performed by ANOVA. Tukey *post hoc* test was used to determine which groups were significant across all treatment groups while Sidak *post hoc* test was used to determine which groups were significant for comparisons of select groups. All results are presented as mean ± SEM. For all statistical tests, results were considered significant at $P < 0.05$.

Results

To assess necuparanib's antitumor potential in pancreatic cancer, we utilized a genetically modified mouse model (GEMM) of the disease. Tumor development in KPFMC (pdx-1-Cre;$Kras^{LSL\text{-}G12D/+}$;$Trp53^{LSL\text{-}R172H/FLOX}$) mice is accelerated compared with KPC mice, and 30 days after birth, all pancreata show evidence of malignant tumor growth (27). As expected, gemcitabine modestly increased survival, although not significantly (from a median survival of 72.5 days with no treatment to 78 days, HR for death = 0.47 (95% confidence interval (CI), 0.17–1.13), $P = 0.088$). While necuparanib did not show a survival benefit as monotherapy, in combination with gemcitabine it significantly increased overall survival compared with saline treatment (to 87 days, HR for death = 0.19; 95% CI, 0.062–0.56; $P < 0.01$) or gemcitabine monotherapy (HR for death = 0.46; 95% CI, 0.21–0.99; $P < 0.05$; Fig. 1A). KPFMC mice develop macrometastases in liver and lungs in about 25% of mice, but up to 85% of all mice have micrometastases (Fig. 1B). Adding necuparanib to gemcitabine treatment significantly decreased the number of mice with soft-tissue metastases compared with gemcitabine treatment alone (15% without metastasis under gemcitabine treatment, 58% without metastasis under treatment with gemcitabine plus necuparanib; $P < 0.05$). Thus, necuparanib significantly increased survival time and reduced metastatic burden when added to chemotherapy treatment in this mouse model.

To further investigate necuparanib's mechanism of action, we developed an *in vitro* model system amenable to assessing necuparanib's multitargeting effects. Embedding the human pancreatic cancer cell line AsPC-1 in a 3D matrix developed round, noninvasive spheroids. AsPC-1 spheroids more than doubled in size over 4 days (from 57,700 ± 2,300 pixels to 129,200 ± 4,300; Fig. 1C). Spheroid growth was reduced by both gemcitabine and necuparanib treatment. Gemcitabine reduced spheroid growth by an average of 38% (70,100 ± 2,100 pixels with saline vs. 43,500 ± 3,000 with gemcitabine; $P < 0.0001$). Necuparanib reduced spheroid size in a dose-dependent manner (Fig. 1C and D). The highest necuparanib dose reduced spheroid size by an average of 50% (35,400 ± 1,600 pixels; $P < 0.0001$ vs. saline). To confirm that the relatively large necuparanib polymer penetrated into spheroids *in vitro*, we imaged spheroids treated with a fluorescently labeled necuparanib derivative (Fig. 1E). Necuparanib penetrated at least 100 nm into the spheroid as evidenced by its intercellular localization (Fig. 1E, arrowheads) and was also taken up by some tumor cells (Fig. 1E, arrows). Thus, necuparanib successfully penetrated the tumor spheroids and affected the tumor cells directly.

To more closely mimic the complex *in vivo* tumor microenvironment, we included a second cell type in our spheroid cultures. *In vivo*, orthotopic injection of the AsPC-1 cell line produces invasive pancreatic tumors (28) but *in vitro*, the AsPC-1 spheroids were noninvasive, suggesting that interactions with at least one other cell type mediate invasive tumor behavior. Pancreatic stellate cells (PSC), the most prevalent pancreatic stromal cells, are one cell type thought to mediate tumor invasion (8, 9, 29). Following incorporation of PSCs into the AsPC-1 spheroids, the coculture spheroids became invasive and developed multiple bud-like protrusions (Fig. 2A), similar to structures reported in other invasive tumor models (30). Coculturing tumor cells with PSCs has also been shown to more closely mimic human pancreatic tumors (31, 32). These invasive buds were composed primarily of tumor cells while PSCs were mostly located in the spheroid center (Supplementary Fig. S1A). Tumor cell invasion could not be induced by the addition of PSC-conditioned media to tumor spheroids (Supplementary Fig. S1B), suggesting that close cell-to-cell contact was necessary. The formation of invasive budding was also largely dependent on the presence of the 3D matrix (Supplementary Fig. S1C). Thus, the addition of PSCs to our tumor spheroid cultures induced invasive behavior of the tumor cells.

We next tested the effects of gemcitabine and necuparanib on the invasive coculture spheroids. As the signature of invasive behavior in our system is a marked change in spheroid morphology, we quantified spheroid shape as a surrogate for invasion (22). Invasive budding decreases circularity. Gemcitabine decreased coculture spheroid growth by an average of 45% (253,400 ± 8,700 pixels without treatment vs. 139,400 ± 2,300 pixels with gemcitabine; $P < 0.0001$; Fig. 2A and B). While gemcitabine treatment decreased the size of the invasive buds, it did not change their presence or number, leaving spheroid circularity unchanged (0.35 ± 0.02 A.U. without treatment and 0.43 ± 0.03 A.U. with treatment, not significant (N.S.); Fig. 2B). However,

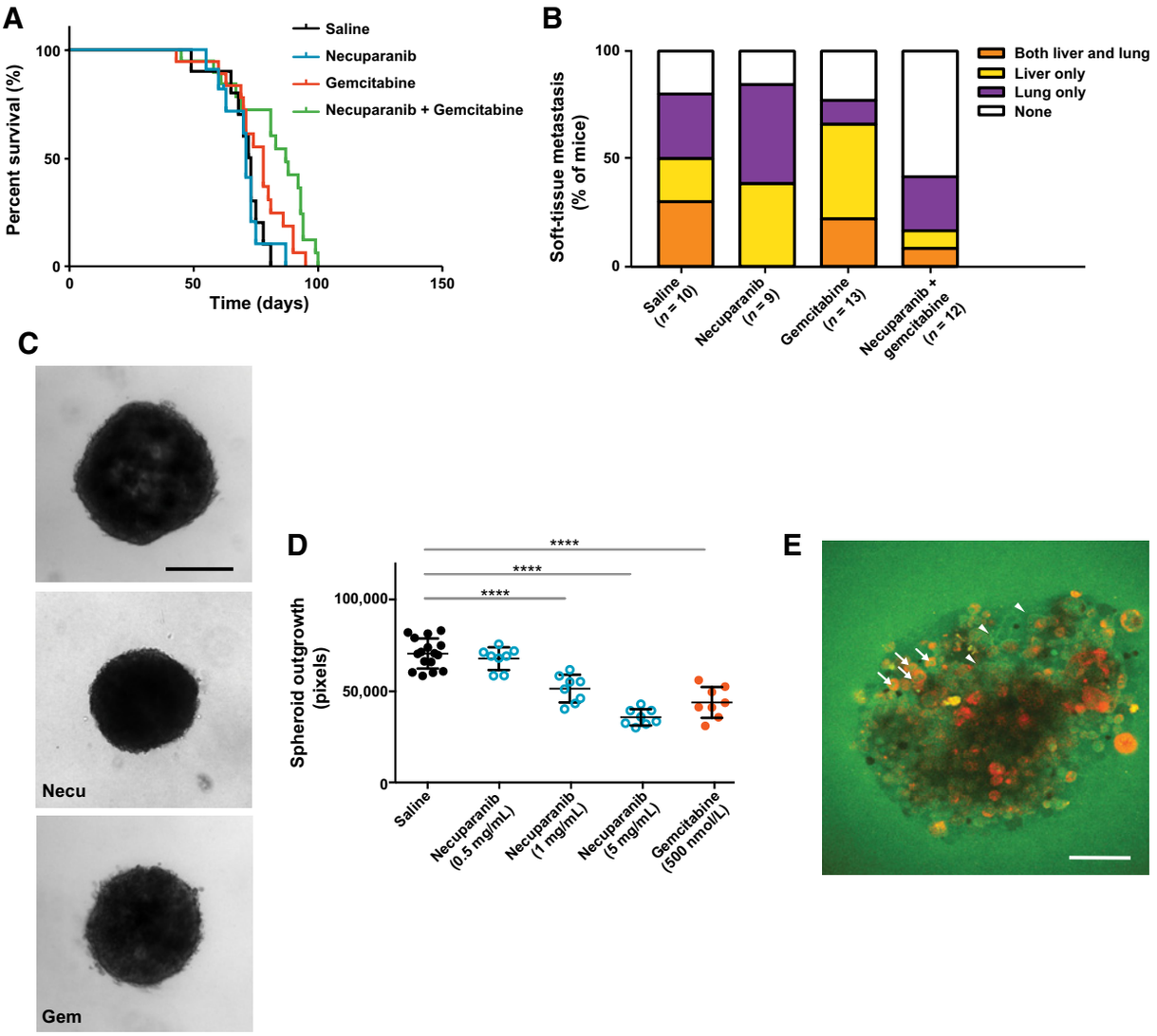

Figure 1.

Necuparanib reduced tumor burden *in vivo* and tumor spheroid size in a 3D *in vitro* model. **A,** KPFMC mice treated with saline or necuparanib (Necu; 40 mg/kg/day) and saline or gemcitabine (Gem; 50 mg/kg/twice weekly) started on day 30. Treatment with necuparanib + gemcitabine significantly extended survival in KPFMC mice over vehicle control ($P < 0.01$) as well as gemcitabine monotherapy ($P < 0.05$). **B,** KPFMC mice treated with necuparanib + gemcitabine had significantly more mice without metastasis compared with gemcitabine monotherapy ($P < 0.05$). **C,** Representative brightfield images of 3D spheroids. Top, untreated AsPC-1 pancreatic cancer cell line spheroid; middle, AsPC-1 spheroid treated with necuparanib (5 mg/mL); bottom, AsPC-1 spheroid treated with gemcitabine (500 nmol/L). Both treatments decreased spheroid size. Scale bar, 500 μm. **D,** Quantification of spheroid outgrowth, the change in spheroid size during exposure to treatment, in untreated spheroids or spheroids treated with necuparanib or gemcitabine. ****, $P < 0.0001$. **E,** Representative confocal image (5 μm optical slice) of a spheroid composed of AsPC-1 cells (red) treated with fluorescently tagged necuparanib (green) reveals accumulation of necuparanib both intercellularly (arrowheads) and intracellularly (arrows). Scale bar, 100 μm.

necuparanib decreased both the number and size of the invasive buds, resulting in rounder spheroids. Necuparanib reduced spheroid growth on average by 32% (to 172,700 ± 8,400 pixels at 1 mg/mL necuparanib, $P < 0.0001$ vs. no treatment) and increased circularity on average by 37% (to 0.59 ± 0.03 A.U., $P < 0.0001$ vs. no treatment; Fig. 2A and B). When used in combination, the effects of gemcitabine and necuparanib were additive, reducing spheroid growth more than either treatment alone (an average of 59%, to 103,400 ± 5,400 pixels, $P < 0.01$). Invasiveness also decreased in the combination treatment to a level similar to necuparanib treatment alone (circularity of 0.62 ± 0.03 A.U., $P < 0.0001$ vs. no treatment; Fig. 2A and B). Therefore, gemcitabine treatment resulted in smaller spheroids that were still invasive in phenotype, while necuparanib reduced both spheroid size and invasive behavior.

To investigate treatment effects, we processed coculture spheroids to quantify markers of cellular proliferation (Ki67) and apoptosis (TUNEL). Necuparanib reduced cellular proliferation by an average of 67% (31.3 ± 4.5% positive cells without treatment vs. 10.3 ± 3.3% with necuparanib; $P < 0.05$), but did

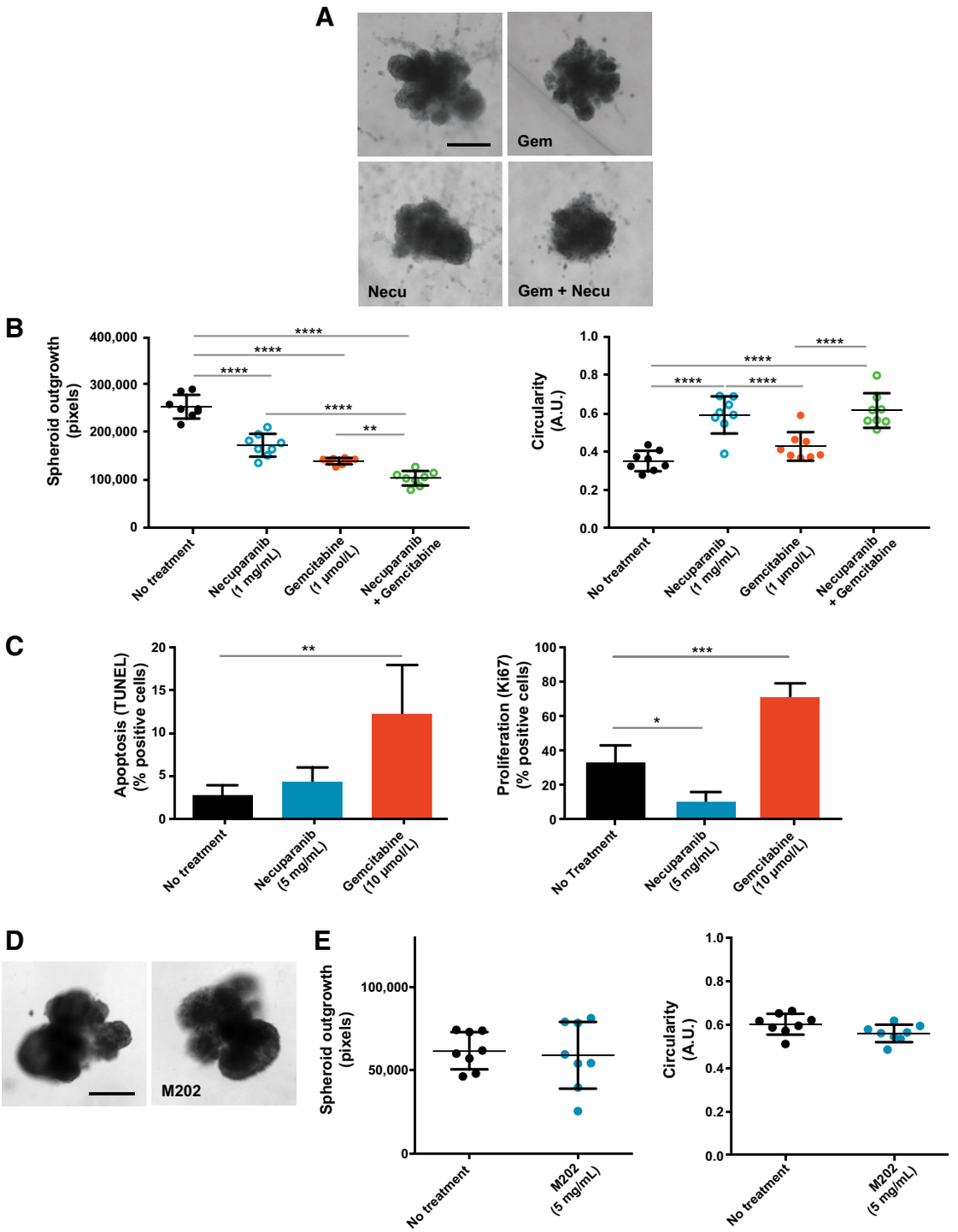

Figure 2.

Necuparanib (Necu) reduced tumor cell proliferation and invasion *in vitro*. **A,** Representative brightfield images of spheroids formed by coculturing AsPC-1 cells and PSCs. Clockwise from top left: untreated cocultured spheroids formed invasive buds; gemcitabine (Gem; 1 μmol/L) reduced spheroid area but not invasive budding; combination treatment (1 mg/mL necuparanib with 1 μmol/L gemcitabine) and necuparanib alone (1 mg/mL) reduced spheroid area and invasiveness. Scale bar, 500 μm. **B,** Quantification of gemcitabine and necuparanib treatment of cocultured spheroids through spheroid area and circularity as a measure of invasion. **, $P < 0.01$; ****, $P < 0.0001$. **C,** Quantification of apoptosis (TUNEL staining) and proliferation (Ki67 staining) of paraffin-embedded sections of cocultured spheroids after treatment. Necuparanib reduced proliferation but did not increase apoptosis; gemcitabine increased apoptosis. *, $P < 0.05$; **, $P < 0.01$. **D,** Representative brightfield images of cocultured spheroids without (left) and with (right) the necuparanib analogue M202 (5 mg/mL). M202 has drastically reduced protein-binding properties compared with necuparanib and it failed to reduce spheroid growth and budding. Scale bar, 500 μm. **E,** Quantification of coculture spheroids treated with M202.

not induce apoptosis (Fig. 2C). Gemcitabine increased apoptosis (4-fold, 2.8 ± 0.4% positive cells without treatment vs. 12.0 ± 2.7% with gemcitabine; $P < 0.01$). Gemcitabine also appeared to increase proliferation although spheroid size decreased under gemcitabine treatment. This is likely an artifact of gemcitabine's well-known ability to arrest cells in different phases of the S-phase cycle, resulting in positive Ki67 staining and creating the appearance of proliferation (33). The additive reduction in spheroid size by gemcitabine and necuparanib combination treatment may thus be driven by a combination of decreased proliferation by necuparanib and increased apoptosis by gemcitabine.

To determine whether necuparanib's antitumor activity was dependent on its multitargeting protein-binding ability, we tested a structural analogue of necuparanib, M202, in the same coculture system. While necuparanib is highly sulfated, M202 lacks N-sulfation. This lack of N-sulfation drastically inhibits charge-based protein binding as we have previously shown (16). While necuparanib reduced both spheroid growth and invasion, M202 reduced neither spheroid growth (61,800 ± 4,000 pixels without treatment vs. 59,000 ± 7,100 pixels with M202, N.S.) nor invasion (circularity of 0.60 ± 0.02 A.U. without treatment vs. 0.56 ± 0.01 A.U. M202, N.S.; Fig. 2D and E). Without the ability to bind proteins, M202 was inactive, suggesting that charge-based protein binding was essential for necuparanib's activity.

To further characterize the impact of necuparanib's multitargeting protein binding, we performed proteomic analysis on the 3D coculture supernatant using SomaLogic's proteomics platform, allowing us to assess over 1,000 low-abundant proteins (23). Compared with untreated supernatant, the majority of proteins in necuparanib-treated 3D cultures had significantly altered levels (81%, 1,059 of 1310 proteins, $P < 0.05$, corrected for false discovery rate (FDR); Fig. 3A). To compensate for potential necuparanib-driven assay interference, we also analyzed a spike control, with necuparanib added into untreated supernatant after collection. Of the proteins altered by necuparanib treatment, we removed proteins from the analysis if they were not also significantly different from the spike control (64% or 679 of 1,059 proteins were removed, $P > 0.05$, FDR corrected; Fig. 3A). Thus, of the total protein set, 380 proteins (29%, $P < 0.05$ both vs. untreated and vs. spike control, FDR corrected) were found to be altered by necuparanib treatment (Fig. 3A). Many of these proteins are not known to bind heparan sulfate, and likely represent proteins whose expression was altered by necuparanib treatment. Thus, over time, necuparanib treatment altered protein levels in our coculture system beyond its ability to directly bind and sequester heparin-binding proteins.

To characterize the biology represented by this set of altered proteins, we utilized the Gene Ontology Consortium (GO) categories. GO categories are a set of genes and gene products linked to biological functions that can be used to comprehensively model a biologic system (25). We determined that of the nearly 2,600 GO categories containing one or more proteins altered by necuparanib treatment, over 150 of these (6%) contained a significant number of altered proteins ($P < 0.05$). The top 35 altered GO categories ($P < 0.01$) are presented in Table 1. As an example, necuparanib's alteration of the proteomic signature altered many categories related to cell growth and organ development, which was expected considering the important role heparan sulfates play in these pathways (34).

Proteomic analysis also allowed us to explore altered protein levels mediating necuparanib's treatment effects. Necuparanib significantly reduced invasive behavior of tumor cells. As invasive processes are known to be MMP dependent, we examined the MMP family of proteins for altered protein levels. Necuparanib significantly reduced levels of MMP1 (2.3× downregulated in necuparanib treated vs. untreated samples; 95% CI, 1.7–2.8; $P < 0.001$, FDR corrected) and increased the broad MMP inhibitor TIMP3 (9.5× upregulated in necuparanib-treated vs. untreated samples; 95% CI = 5.5–16.5; $P < 0.001$; FDR corrected) in 3D cocultures (Fig. 3B; Supplementary Table S1). Both proteins were altered by necuparanib treatment, but not by the spike control, suggesting that these changes are due to altered protein expression and not simply protein-binding effects. As heparins are known to bind and release TIMP3 from the ECM (35), we confirmed that altered MMP1 and TIMP3 levels were driven by changes in expression and we measured RNA expression in coculture spheroids. Necuparanib significantly increased TIMP3 RNA expression (by 1.5-fold compared with untreated spheroids, $P < 0.01$), but did not significantly change MMP1 expression levels although there was a trend toward decreased expression (a reduction of 0.8-fold; $P = 0.0518$; Fig. 3C). Thus, necuparanib treatment increased TIMP3 levels in our model system, likely by both increased expression and increased release from the ECM.

As measured MMP protein levels do not directly correspond to MMP activity, we first confirmed that MMP activity supported invasive behavior in our coculture system using the synthetic pan-MMP inhibitor GM6001. GM6001 both reduced spheroid size (by an average of 43%, 255,000 ± 50,000 pixels with DMSO control vs. 145,000 ± 18,000 with GM6001, $P < 0.01$) and invasiveness (by an average of 35%, circularity of 0.69 ± 0.03 A.U. with DMSO control vs. 0.80 ± 0.03 A.U with GM6001, $P < 0.05$; Supplementary Fig. S2), confirming that tumor cell invasiveness was at least, in part, dependent on MMP activity. Next, we examined the effect of necuparanib treatment on MMP activity by embedding DQ substrates into the spheroid matrix; DQ substrates become fluorescent upon MMP digestion. Degradation of both DQ-collagen I (by collagenases) and DQ-gelatin (by gelatinases) was reduced with either GM6001 or necuparanib, but not with gemcitabine (fluorescence reduction of DQ-collagen digestion of an average of 50.6% ± 8.6% with necuparanib and 55.5% ± 7.3% with GM6001, $P < 0.0001$; reduction of 15.2 ± 4.0% with gemcitabine, N.S.; DQ-gelatin results were similar; Fig. 3D and E). Thus, necuparanib's inhibition of invasion was dependent at least in part on reduced MMP levels and activity.

To confirm whether our findings of altered MMP protein levels with necuparanib treatment could be observed in patients, we examined plasma from patients treated with necuparanib. Measurable levels of multiple MMPs and TIMP3 have been detected in urine and plasma of patients with pancreatic cancer (36–40). We tested plasma samples obtained from patients with metastatic pancreatic cancer enrolled in a phase II clinical trial of necuparanib, which was composed of two arms: standard of care (SOC, gemcitabine + nab-paclitaxel) and SOC plus necuparanib (Fig. 4A). Linear mixed effects (LME) models were used to assess changes in MMP expression over time and calculate P values. We tested several MMPs shown to be involved in pancreatic cancer development (MMP1, MMP2, MMP7, and MMP9) as well as TIMP3. Neither MMP1 nor MMP7 changed during treatment (Supplementary Fig. S3), but both MMP2 and MMP9 were altered over time in each treatment arm (in patients receiving SOC plus necuparanib MMP2 increased from 2.29 ± 0.3 ng/mg to 3.38 ± 0.4 ng/mg during treatment, $P < 0.0001$ and MMP9 decreased

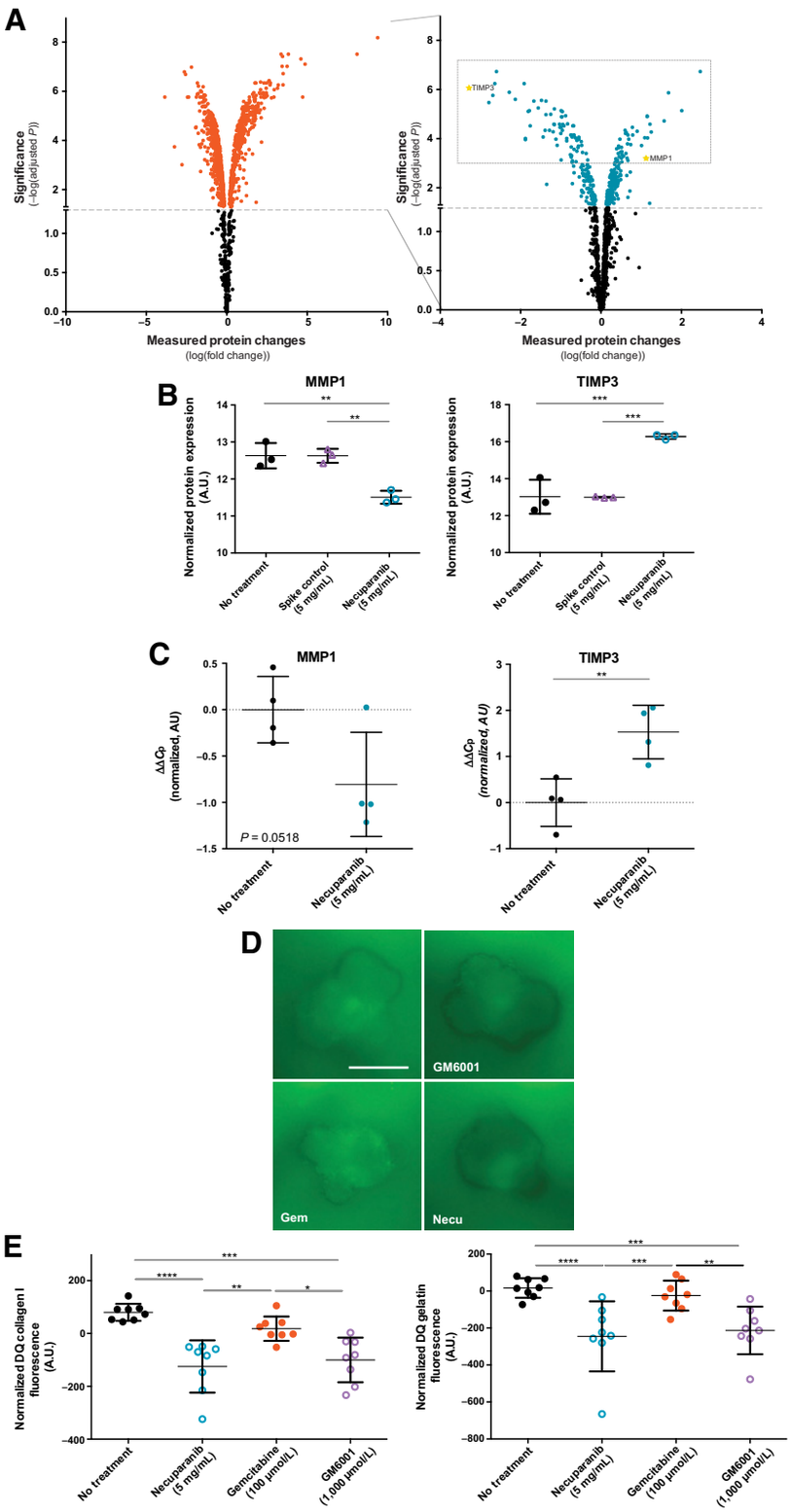

Figure 3.

Necuparanib (Necu) altered the protein expression and reduced MMP activity in the coculture spheroids. **A,** Left, quantification of the significance and fold change of protein levels altered by necuparanib treatment compared with no treatment. Nearly 80% of proteins were significantly altered (red circles, $P < 0.05$, FDR corrected). Right, quantification of the significance and fold change of proteins altered by necuparanib treatment when compared with a spike control. The majority of proteins (black circles, $P > 0.05$, FDR corrected) were not significantly different from the spike control, and may represent proteins altered by assay interference. Proteins that were both significantly altered by necuparanib treatment and significantly different from the spike control (blue circles, $P < 0.05$, FDR corrected) likely represent proteins with altered expression levels; rectangle displays the subset of significantly altered proteins ($P < 0.001$) listed in Supplementary Table S1. **B,** Quantification of protein levels of two proteins found to be significantly altered by necuparanib treatment, MMP1, and the broad MMP inhibitor TIMP3. Both proteins are altered by necuparanib treatment, but are unchanged in the spike control. **, $P < 0.01$; ***, $P < 0.001$. **C,** Quantification of the relative RNA expression of MMP-1 and TIMP3 in coculture spheroids with and without 5 mg/mL necuparanib treatment. **, $P < 0.01$. **D,** Overlay of representative brightfield and fluorescent images of coculture spheroids embedded in a matrix doped with DQ collagen I. Upon digestion with MMPs, DQ collagen I became fluorescent (green). Clockwise from top left, untreated coculture spheroids displayed higher MMP activity near PSC clusters; the pan MMP-inhibitor GM6001 (1,000 μmol/L) reduced MMP activity; necuparanib (5 mg/mL) reduced MMP activity; gemcitabine (Gem; 100 μmol/L) did not alter MMP activity. Scale bar, 500 μm. **E,** Quantification of fluorescent images taken of coculture spheroids embedded in a matrix doped with DQ collagen (left) and DQ gelatin (right). As fluorescence was normalized against matrix background, negative values reflect spheroids that were darker than their surroundings. *, $P < 0.05$; **, $P < 0.01$; ***, $P < 0.001$; ****, $P < 0.0001$.

from 1.80 ± 0.2 ng/mg to 1.10 ± 0.3 ng/mg, $P < 0.001$; results for SOC alone are similar; Fig. 4B). However, TIMP3 levels increased over time for patients who received the combination of SOC plus necuparanib (increased from an average of 0.278 ± 0.04 ng/mg to 0.330 ± 0.05 ng/mg during treatment), while TIMP3 levels slightly decreased over the treatment period in patients on SOC alone (decreased from an average of 0.198 ± 0.02 ng/mg to 0.178 ± 0.02 ng/mg at the end of treatment; Fig. 4B). The LME

Table 1. GO Categories significantly altered by necuparanib treatment

GO Category ID	GO Category description	Annotated proteins	Significantly altered proteins	*P*
GO:0090257	Regulation of muscle system process	36	21	0.0005
GO:0003012	Muscle system process	51	26	0.0018
GO:0001889	Liver development	27	16	0.0019
GO:0010833	Telomere maintenance via telomere lengthening	10	8	0.0019
GO:0061008	Hepatobiliary system development	27	16	0.0019
GO:1900182	Positive regulation of protein localization to nucleus	47	24	0.0026
GO:0034504	Protein localization to nucleus	73	34	0.0027
GO:0014013	Regulation of gliogenesis	19	12	0.0035
GO:0016458	Gene silencing	17	11	0.0039
GO:0016049	Cell growth	110	47	0.0041
GO:1900180	Regulation of protein localization to nucleus	56	27	0.0041
GO:0000060	Protein import into nucleus translocation	15	10	0.0044
GO:0007399	Nervous system development	298	111	0.0045
GO:0046824	Positive regulation of nucleocytoplasmic transport	46	23	0.0045
GO:0003013	Circulatory system process	83	37	0.0046
GO:0008015	Blood circulation	83	37	0.0046
GO:0044085	Cellular component biogenesis	259	98	0.0046
GO:0017038	Protein import	70	32	0.0052
GO:0051961	Negative regulation of nervous system development	49	24	0.0053
GO:0003018	Vascular process in circulatory system	34	18	0.0055
GO:0090316	Positive regulation of intracellular protein transport	57	27	0.0056
GO:0022607	Cellular component assembly	252	95	0.0061
GO:0048468	Cell development	304	112	0.0066
GO:0006913	Nucleocytoplasmic transport	82	36	0.007
GO:0051169	Nuclear transport	82	36	0.007
GO:0007492	Endoderm development	18	11	0.0074
GO:0035051	Cardiocyte differentiation	25	14	0.0074
GO:0040029	Regulation of gene expression epigenetic	18	11	0.0074
GO:0048699	Generation of neurons	215	82	0.0079
GO:0006606	Protein import into nucleus	64	29	0.009
GO:0044744	Protein targeting to nucleus	64	29	0.009
GO:1902593	Single-organism nuclear import	64	29	0.009
GO:0051960	Regulation of nervous system development	140	56	0.0097
GO:0002474	Antigen processing and presentation of peptide antigen via MHC class I	14	9	0.0099
GO:0032570	Response to progesterone	14	9	0.0099

model showed that these changes in TIMP3 levels were significantly different between the two arms ($P = 0.03$ for the interaction between time and treatment). While the significant increase in TIMP3 seen in patient plasma was based on just a few patients, it confirms our *in vitro* findings. The increase in TIMP3 plasma levels was suggestive of biological activity *in vivo* for necuparanib, and may be a biomarker of necuparanib's functional activity.

Discussion

Necuparanib, a heparin mimetic, acts as a multitargeting therapeutic. Here we demonstrated that necuparanib's multitargeting abilities reduced tumor growth, mediated tumor–stromal interactions, and altered multiple cellular processes in *in vitro* and *in vivo* models of pancreatic cancer.

Heparins and other anticoagulants have been prescribed to oncology patients for decades to prevent venous thromboembolism (VTE), a comorbidity of cancer. As the hemostatic system has also been shown to play a role in tumor development and progression, multiple clinical trials have examined whether heparin therapy adds to the efficacy of chemotherapeutics beyond VTE prevention; although there has been some evidence of benefit, dosing has been limited due to heparin's anticoagulant activity (41). Necuparanib was designed, in part, to build upon the clinical benefit of heparin therapy, with reduced anticoagulation properties to enable higher dosing levels. In a mouse model of breast cancer, we previously found that necuparanib treatment added to the efficacy of the chemotherapy docetaxel (16). Here, we extended these findings, showing that necuparanib treatment not only added to the efficacy of gemcitabine *in vitro*, but also acted directly on pancreatic tumor cells. Necuparanib reduced tumor cell proliferation *in vitro* and added to the ability of gemcitabine to reduce tumor spheroid size in a 3D model. Importantly, necuparanib also altered tumor–stromal interactions, reducing tumor invasion in our 3D model. Invasion was reduced only by necuparanib treatment and not by gemcitabine. These results are in agreement with previous preclinical studies, which found that heparins were able to reduce tumor growth, although only when given at high doses over long periods of time (42).

Endogenous heparan sulfates and the proteins that bind to them have been shown to govern multiple pathways in the development and metastasis of cancer (43, 44). Previously, we demonstrated that necuparanib can compete with these pathways, binding and sequestering heparin-binding proteins, and disrupting pathways such as angiogenesis and chemotaxis (16). Using proteomics on our 3D model system, we expanded these findings here to show that necuparanib treatment alters hundreds of proteins and their associated cellular functions. As only a fifth of the altered proteins (85 of the 380 altered) are known to be heparin-binding, our results suggest that over time, necuparanib treatment alters protein expression, changing protein levels

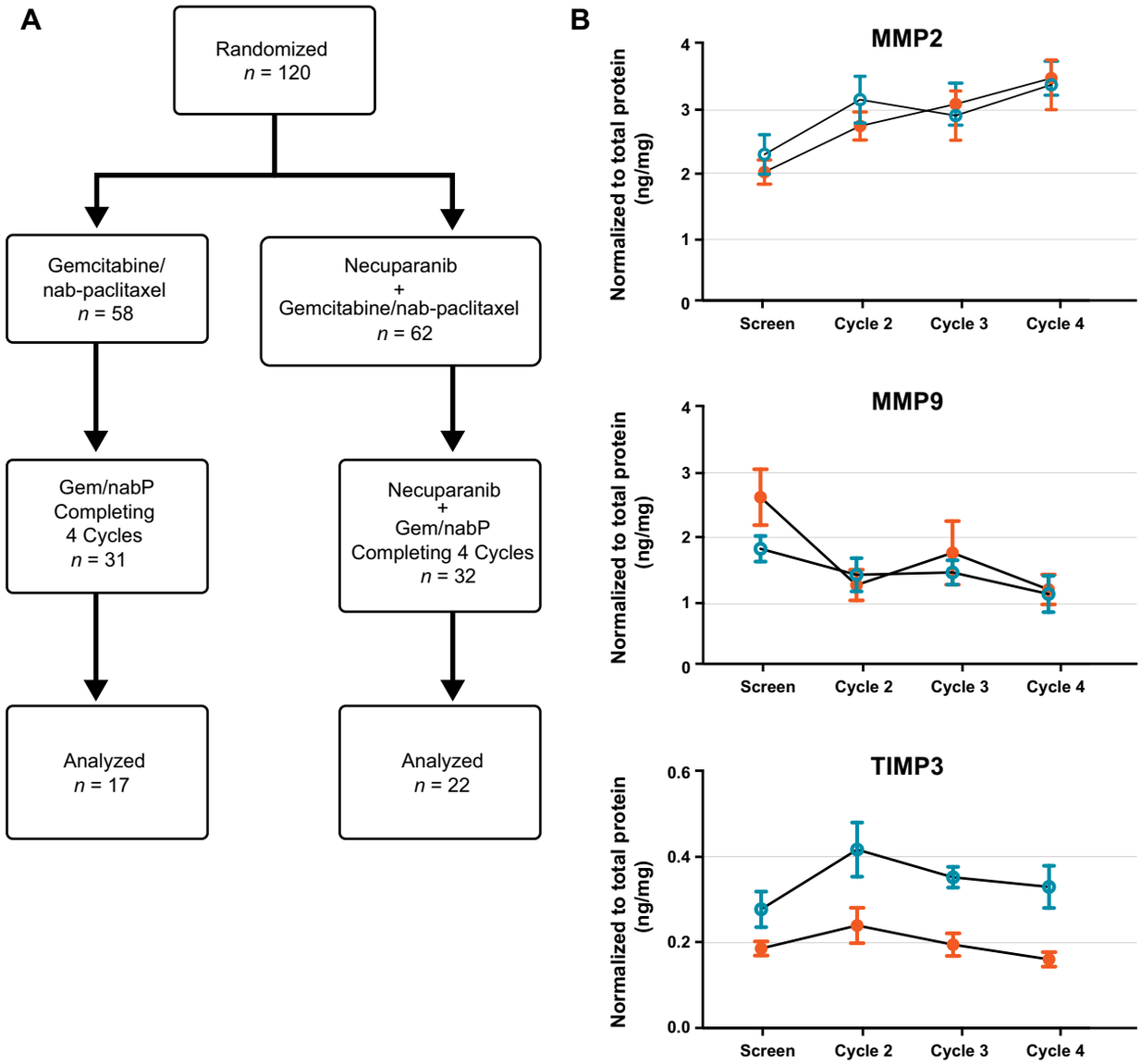

Figure 4.

TIMP3 protein levels increased in the plasma of patients treated with SOC plus necuparanib and decreased slightly in the SOC only group. **A,** Overview of clinical trial treatment arms and derivation of representative patient samples. **B,** Quantification of MMP2, MMP9 and TIMP3 levels in patients' plasma measured over 4 cycles of treatment (28-day cycles) of either SOC alone (red) or SOC plus necuparanib (blue). Protein levels were normalized to total plasma protein content, and protein levels at each time point were averaged across treatment arms. While protein levels for both MMP2 and MMP9 showed identical changes in protein expression for both treatment arms, only patients receiving necuparanib as part of their treatment regime exhibited an increase in TIMP3 protein expression over time and when compared with SOC alone ($P < 0.05$ for the interaction term between time and treatment from a linear mixed effects (LME) model).

beyond its immediate binding partners. Indeed, we confirmed that necuparanib treatment increased TIMP3 expression *in vitro*. Furthermore, we linked these altered proteins to hundreds of significantly impacted GO categories (Table 1), many of which (cell development (34), vascular processes (45), muscle development (46) and nuclear processes (47)) have been shown to have heparan sulfates play key signaling roles.

Our proteomic data and supporting experimental evidence demonstrated that necuparanib's impact on protein expression represents a broad restriction on the pathways that drive the development of cancer. Using pathways adapted from the "hallmarks of cancer" identified by Hanahan and Weinberg (48), we grouped significantly impacted GO categories into cancer-driving pathways (Supplementary Table S2; Fig. 5). Pathways were adapted from the hallmarks of cancer as they are hypothesized to fully describe the diversity in pathologic biology present in the tumor and tumor microenvironment (48). For example, cell projection assembly (GO category 0030031) and chemotaxis (0006935) were grouped with other altered categories into the "invasion and metastasis" pathway (Supplementary Table S2). Of

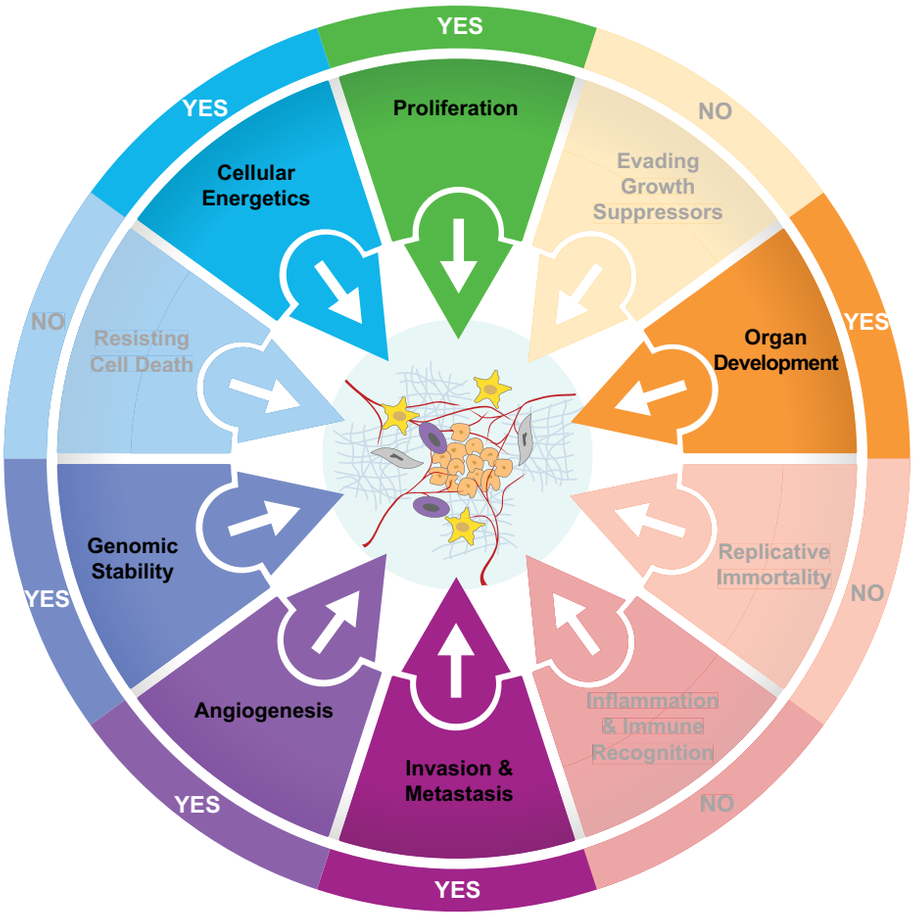

Figure 5.
Necuparanib treatment altered multiple cancer-promoting pathways. Cancer-driving pathways figure adapted from the Hallmarks of Cancer: the next generation (43). Pathways impacted by necuparanib treatment highlighted by "YES."

the 10 cancer-driving pathways adapted from Hanahan and Weinberg, proteomic analysis showed that necuparanib treatment significantly impacted ($P < 0.05$) biological functions related to six of those: proliferation, organ development, invasion and metastasis, angiogenesis, genomic stability, and cellular energetics (Supplementary Table S2; Fig. 5). Of these six, our *in vitro* and *in vivo* results here confirmed necuparanib reduced proliferation and invasion and metastasis; previously, we also confirmed a reduction in other metastatic models and in angiogenesis (16). Together, data presented herein suggest that as necuparanib treatment blocks multiple cancer-driving pathways, it may be broadly effective across a range of cancers.

Necuparanib altered proteins linked to invasion and metastasis in our 3D model and reduced metastasis *in vivo* in a mouse model of pancreatic cancer. To create an invasive 3D tumor model, we found that human pancreatic cancer cell lines required the addition of another cell type. Tumor cells cocultured with PSCs, the most prevalent cell type found in the stromal compartment of human pancreatic tumors, confirmed the importance of PSCs in accurately modeling pancreatic tumor development and pathology as tumor spheroids became invasive (10, 31). Mechanistically, necuparanib's ability to disrupt PSC–tumor signaling and inhibit tumor cell invasion was shown to be driven in part by the alteration of protein levels and activity of members of the MMP family. Necuparanib treatment reduced MMP1 protein levels and increased protein levels of TIMP3, a broad MMP inhibitor in our 3D coculture model; necuparanib treatment also increased TIMP3 expression. Furthermore, we found that the increased levels of TIMP3 seen *in vitro* were also found in the plasma of patients treated with SOC plus necuparanib. This *in vivo* increase confirms that the proteomic signature of necuparanib treatment *in vitro* was representative of human pancreatic tumor biology. Necuparanib's ability to increase TIMP3 levels in patients may serve as an important treatment marker, and suggests necuparanib has the potential to inhibit MMP activity and MMP-driven pathology in other diseases.

As necuparanib advanced into the clinic, phase I demonstrated acceptable patient tolerability of necuparanib in combination with nab-paclitaxel and gemcitabine therapy (49). However, a routine interim analysis of the phase II study in patients with metastatic pancreatic cancer revealed that adding necuparanib to the SOC did not sufficiently increase therapeutic efficacy to warrant continuation of the study. As many proven therapies have failed to improve survival in metastatic pancreatic cancer (50, 51), we remain hopeful that necuparanib may be a promising therapeutic opportunity for earlier stage pancreatic cancer and other cancers.

In summary, necuparanib, a multitargeting agent able to bind and sequester multiple proteins, was shown to act directly on the growth and development of pancreatic cancer in *in vitro* and *in vivo* models of the disease. Our results suggest that necuparanib can add to the efficacy of many common chemotherapeutics, acting

broadly to simultaneously restrict multiple cancer-driving pathways. Furthermore, necuparanib's ability to restrict MMP activity *in vitro* and alter TIMP3 protein levels *in vitro* and in patients suggests that necuparanib can reduce MMP activity *in vivo*. Our results demonstrate that necuparanib is a promising multitargeting cancer therapeutic with the potential to impact multiple cancers.

Disclosure of Potential Conflicts of Interest

A. MacDonald is a postdoctoral associate at Momenta Pharmaceuticals. V. Farutin has ownership interest (including stock, patents, etc.) in Momenta Pharmaceuticals, Inc. E. Cochran is an associate scientist and has ownership interest (including stock, patents, etc.) in Momenta Pharmaceuticals. M. Lolkema reports receiving a commercial research grant from Momenta Pharmaceuticals. B.C. Schultes is a senior director at Momenta Pharmaceuticals. S. Krause has ownership interest (including stock, patents, etc.). No potential conflicts of interest were disclosed by the other authors.

Disclaimer

The funding source does not compromise the objectivity or validity of the research, analyses, and interpretations presented in the paper.

Authors' Contributions

Conception and design: A. MacDonald, M. Priess, M. Lolkema, B.C. Schultes, S. Krause
Development of methodology: A. MacDonald, M. Priess, L. Zhang, M. Lolkema, S. Krause
Acquisition of data (provided animals, acquired and managed patients, provided facilities, etc.): A. MacDonald, M. Priess, J. Curran, I. Oosterom, C.L. Chu, E. Cochran, L. Zhang, K. Getchell, M. Lolkema, S. Krause
Analysis and interpretation of data (e.-g., statistical analysis, biostatistics, computational analysis): A. MacDonald, J. Curran, J. Guess, V. Farutin, E. Cochran, L. Zhang, M. Lolkema, S. Krause
Writing, review, and/or revision of the manuscript: A. MacDonald, J. Guess, V. Farutin, C.L. Chu, L. Zhang, M. Lolkema, B.C. Schultes, S. Krause
Study supervision: C.L. Chu, M. Lolkema, B.C. Schultes, S. Krause

Acknowledgments

The authors would like to thank Sucharita Roy for the initial design of the compounds, John Schaeck for labeling of the compounds, and Savannah Moore and Guilin Wang for their help in performing supporting assays. The authors are grateful to the Wyss Institute for Biologically Inspired Engineering for allowing us to utilize their confocal microscope. The authors are thankful to Bill Avery, Tanmoy Ganguly, and Joel Pradines for critically reading the manuscript and helpful discussions. M.P. Lolkema has received a Dutch Cancer Foundation Fellowship grant (UU2008-4380) to support this work. The rest of the study is funded by Momenta Pharmaceuticals.

The costs of publication of this article were defrayed in part by the payment of page charges. This article must therefore be hereby marked *advertisement* in accordance with 18 U.S.C. Section 1734 solely to indicate this fact.

Received April 20, 2018; revised September 6, 2018; accepted November 2, 2018; published first November 6, 2018.

References

1. Jemal A, Siegel R, Ward E, Murray T, Xu J, Thun MJ. Cancer statistics, 2007. CA Cancer J Clin 2007;57:43–66.
2. Siegel R, Naishadham D, Jemal A. Cancer statistics, 2017. CA Cancer J Clin 2017;67:7–30.
3. Stathis A, Moore MJ. Advanced pancreatic carcinoma: current treatment and future challenges. Nat Rev Clin Oncol 2010;7:163–72.
4. Oberstein PE, Olive KP. Pancreatic cancer: why is it so hard to treat? Therap Adv Gastroenterol 2013;6:321–37.
5. Garrido-Laguna I, Hidalgo M. Pancreatic cancer: from state-of-the-art treatments to promising novel therapies. Nat Rev Clin Oncol 2015;12:319–34.
6. Rahib L, Smith BD, Aizenberg R, Rosenzweig AB, Fleshman JM, Matrisian LM. Projecting cancer incidence and deaths to 2030: the unexpected burden of thyroid, liver, and pancreas cancers in the United States. Cancer Res 2014;74:2913–21.
7. Neesse A, Algul H, Tuveson DA, Gress TM. Stromal biology and therapy in pancreatic cancer: a changing paradigm. Gut 2015;64:1476–84.
8. Feig C, Gopinathan A, Neesse A, Chan DS, Cook N, Tuveson D. The pancreas cancer microenvironment. Clin Cancer Res 2012;18:4266–76.
9. Phillips P. Pancreatic stellate cells and fibrosis. In: Grippo PJ, Munshi HG, editors. Pancreatic cancer tumor microenvironment. Trivandrum, India: Transworld Research Network; 2012. p.29–53.
10. Apte MV., Park S, Phillips PA, Santucci N, Goldstein D, Kumar RK, et al. Desmoplastic reaction in pancreatic cancer: role of pancreatic stellate cells. Pancreas 2004;29:179–87.
11. Rhim AD, Oberstein PE, Thomas DH, Mirek ET, Palermo CF, Sastra SA, et al. Stromal elements act to restrain, rather than support, pancreatic ductal adenocarcinoma. Cancer Cell 2014;25:735–47.
12. Özdemir BC, Pentcheva-Hoang T, Carstens JL, Zheng X, Wu C-C, Simpson TR, et al. Depletion of carcinoma-associated fibroblasts and fibrosis induces immunosuppression and accelerates pancreas cancer with reduced survival. Cancer Cell 2014;25:719–34.
13. Bahrami A, Khazaei M, Bagherieh F, Ghayour-Mobarhan M, Maftouh M, Hassanian SM, et al. Targeting stroma in pancreatic cancer: promises and failures of targeted therapies. J Cell Physiol 2017;232:2931–7.
14. Kota J, Hancock J, Kwon J, Korc M. Pancreatic cancer: Stroma and its current and emerging targeted therapies. Cancer Lett 2017;391:38–49.
15. Sherman MH, Yu RT, Engle DD, Ding N, Atkins AR, Tiriac H, et al. Vitamin D receptor-mediated stromal reprogramming suppresses pancreatitis and enhances pancreatic cancer therapy. Cell 2014;159:80–93.
16. Zhou H, Roy S, Cochran E, Zouaoui R, Chu CL, Duffner J, et al. M402, a novel heparan sulfate mimetic, targets multiple pathways implicated in tumor progression and metastasis. PLoS One 2011;6:e21106.
17. Balakrishnan A, Patel B, Sieber S, Chen D, Pachikara N, Zhong G, et al. Metalloprotease inhibitors GM6001 and TAPI-0 inhibit the obligate intracellular human pathogen *Chlamydia trachomatis* by targeting peptide deformylase of the bacterium. J Biol Chem 2006;281:16691–9.
18. Olive KP, Tuveson DA, Ruhe ZC, Yin B, Willis NA, Bronson RT, et al. Mutant p53 gain of function in two mouse models of Li-Fraumeni syndrome. Cell 2004;119:847–60.
19. Hingorani SR, Wang L, Multani AS, Combs C, Deramaudt TB, Hruban RH, et al. Trp53R172H and KrasG12D cooperate to promote chromosomal instability and widely metastatic pancreatic ductal adenocarcinoma in mice. Cancer Cell 2005;7:469–83.
20. Liang C, Shi S, Meng Q, Liang D, Ji S, Zhang B, et al. Complex roles of the stroma in the intrinsic resistance to gemcitabine in pancreatic cancer: where we are and where we are going. Exp Mol Med 2017;49:1–10.
21. Abràmoff MD, Magalhães PJ. Image processing with ImageJ. Biophotonics Int 2004;11:36–42.
22. Cox EP. A method of assigning numerical and percentage values to the degree of roundness of sand grains. J Paleontol 1927;1:179–83.
23. Gold L, Ayers D, Bertino J, Bock C, Bock A, Brody EN, et al. Aptamer-based multiplexed proteomic technology for biomarker discovery. PLoS One 2010;5:e15004.
24. Ritchie ME, Phipson B, Wu D, Hu Y, Law CW, Shi W, et al. *limma* powers differential expression analyses for RNA-sequencing and microarray studies. Nucleic Acids Res 2015;43:e47.
25. Alexa A, Rahnenfuhrer J. topGO: Enrichment analysis for gene ontology. R package version 2.28.0; 2016. Available from: www.bioconductor.org
26. Bates D, Mächler M, Bolker BM, Walker SC. Fitting linear mixed-effects models using lme4. J Stat Softw 2015;67:1–48.
27. Beerling E, Oosterom I, Voest E, Lolkema M, van Rheenen J. Intravital characterization of tumor cell migration in pancreatic cancer. IntraVital 2016;5:e1261773-1–8.

28. Tan MH, Chu TM. Characterization of the tumorigenic and metastatic properties of a human pancreatic tumor cell line (AsPC-1) implanted orthotopically into nude mice. Tumour Biol 1985;6:89–98.
29. von Ahrens D, Bhagat TD, Nagrath D, Maitra A, Verma A. The role of stromal cancer-associated fibroblasts in pancreatic cancer. J Hematol Oncol 2017;10:76.
30. Vinci M, Box C, Eccles SA. Three-dimensional (3D) tumor spheroid invasion assay. J Vis Exp 2015;99:e52686.
31. Hwang RF, Moore T, Arumugam T, Ramachandran V, Amos KD, Rivera A, et al. Cancer-associated stromal fibroblasts promote pancreatic tumor progression. Cancer Res 2008;68:918–26.
32. Öhlund D, Handly-Santana A, Biffi G, Elyada E, Almeida AS, Ponz-Sarvise M, et al. Distinct populations of inflammatory fibroblasts and myofibroblasts in pancreatic cancer. J Exp Med 2017;214:579–96.
33. Montano R, Thompson R, Chung I, Hou H, Khan N, Eastman A. Sensitization of human cancer cells to gemcitabine by the Chk1 inhibitor MK-8776: cell cycle perturbation and impact of administration schedule in vitro and in vivo. BMC Cancer 2013;13:604.
34. Bülow HE, Hobert O. The molecular diversity of glycosaminoglycans shapes animal development. Annu Rev Cell Dev Biol 2006;22:375–407.
35. Yu WH, Yu SSC, Meng Q, Brew K, Woessner JF. TIMP-3 binds to sulfated glycosaminoglycans of the extracellular matrix. J Biol Chem 2000;275: 31226–32.
36. Kuhlmann KFD, Van Till JWO, Boermeester MA, De Reuver PR, Tzvetanova ID, Offerhaus GJA, et al. Evaluation of matrix metalloproteinase 7 in plasma and pancreatic juice as a biomarker for pancreatic cancer. Cancer Epidemiol Biomarkers Prev 2007;16:886–91.
37. Nagao Y, Hisaoka M, Matsuyama A, Kanemitsu S, Hamada T, Fukuyama T, et al. Association of microRNA-21 expression with its targets, PDCD4 and TIMP3, in pancreatic ductal adenocarcinoma. Mod Pathol 2012;25: 112–21.
38. Jackson HW, Defamie V, Waterhouse P, Khokha R. TIMPs: Versatile extracellular regulators in cancer. Nat Rev Cancer 2017;17:38–53.
39. Wild A, Ramaswamy A, Langer P, Celik I, Fendrich V, Chaloupka B, et al. Frequent methylation-associated silencing of the tissue inhibitor of metalloproteinase-3 gene in pancreatic endocrine tumors. J Clin Endocrinol Metab 2003;88:1367–73.
40. Jones LE, Humphreys MJ, Campbell F, Neoptolemos JP, Boyd MT. Comprehensive analysis of matrix metalloproteinase and tissue inhibitor expression in pancreatic cancer: increased expression of matrix metalloproteinase-7 predicts poor survival. Clin Cancer Res 2004;10: 2832–45.
41. García-Escobar I, Beato-Zambrano C, Muñoz Langa J, Brozos Vázquez E, Obispo Portero B, Gutiérrez-Abad D, et al. Pleiotropic effects of heparins: does anticoagulant treatment increase survival in cancer patients? Clin Transl Oncol 2018;20:1097–108.
42. Niers TMH, Klerk CPW, DiNisio M, Van Noorden CJF, Büller HR, Reitsma PH, et al. Mechanisms of heparin induced anti-cancer activity in experimental cancer models. Crit Rev Oncol Hematol 2007;61: 195–207.
43. Sasisekharan R, Shriver Z, Venkataraman G, Narayanasami U. Roles of heparan-sulphate glycosaminoglycans in cancer. Nat Rev Cancer 2002;2: 521–8.
44. Knelson EH, Nee JC, Blobe GC. Heparan sulfate signaling in cancer. Trends Biochem Sci 2014;39:277–88.
45. Iozzo R, Antonio JS. Heparan sulfate proteoglycans: heavy hitters in the angiogenesis arena. J Clin Invest 2001;108:349–55.
46. Bink RJ, Habuchi H, Lele Z, Dolk E, Joore J, Rauch GJ, et al. Heparan sulfate 6-O-sulfotransferase is essential for muscle development in zebrafish. J Biol Chem 2003;278:31118–27.
47. Hsia E, Richardson TP, Nugent MA. Nuclear localization of basic fibroblast growth factor is mediated by heparan sulfate proteoglycans through protein kinase C signaling. J Cell Biochem 2003;88:1214–25.
48. Hanahan D, Weinberg RA. Hallmarks of cancer: the next generation. Cell 2011;144:646–74.
49. O'Reilly EM, Mahalingam D, Roach JM, Schultes BC, Rosano ME, Miller PJ, et al. Safety, pharmacokinetics, pharmacodynamics, and antitumor activity of necuparanib combined with nab-paclitaxel and gemcitabine in patients with metastatic pancreatic cancer: Phase 1 results. Oncologist 2017;22: 1429–e139.
50. Adamska A, Domenichini A, Falasca M. Pancreatic ductal adenocarcinoma: current and evolving therapies. Int J Mol Sci 2017;18:1338.
51. Welch S, Moore M. Combination chemotherapy in advanced pancreatic cancer: time to raise the white flag? J Clin Oncol 2007;25:2159–61.